Local field potentials primarily reflect inhibitory neuron activity in human and monkey cortex

Bartosz Teleńczuk[a,*], Nima Dehghani[b,c], Michel Le Van Quyen[d], Sydney S. Cash[e], Eric Halgren[f], Nicholas G. Hatsopoulos[g], Alain Destexhe[a]

[a] *Unité de Neurosciences, Information & Complexité, Centre National de la Recherche Scientifique, 91198 Gif-sur-Yvette, France*
[b] *Wyss Institute for Biologically-Inspired Engineering, Harvard University, Boston, USA*
[c] *New England Complex Systems Institute, Cambridge, USA*
[d] *L'Institut du Cerveau et de la Moelle Épinière, UMRS 1127, CNRS UMR 7225, Hôpital de la Pitié-Salpêtrière, Paris, France*
[e] *Department of Neurology, Massachusetts General Hospital and Harvard Medical School, USA.*
[f] *Multimodal Imaging Laboratory, Departments of Neurosciences and Radiology, University of California San Diego, USA.*
[g] *Department of Organismal Biology and Anatomy, Committee on Computational Neuroscience, University of Chicago, USA*

Abstract

The local field potential (LFP) is generated by large populations of neurons, but unitary contribution of spiking neurons to LFP is not well characterized. We investigated this contribution in multi-electrode array recordings from the cerebral cortex of human and monkey by calculating the spike-triggered LFP average (st-LFP). The resulting st-LFPs were dominated by broad spatio-temporal components due to on-going activity, synaptic inputs and recurrent connectivity. To observe the local field of a single spike we applied spatial filtering. The filtered st-LFPs were limited to an area of 800 μm from the neuron, and propagated at axonal speed, which is consistent with their unitary nature. In addition, we discriminated between putative inhibitory and excitatory neurons and found that the former dominated this unitary LFP contribution, consistently with previous findings in hippocampal slices. Thus, in human and monkey cortex, the LFP may primarily reflect inhibitory neuron activity.

1. Introduction

The information in neural systems is distributed across a large number of neurons. In order to understand how it is encoded, processed and transformed into actions, we need to monitor activities of significant fraction of the neuronal population (Georgopoulos et al., 1986). A popular measure of the population activity is the local field potential (LFP), which represents

*Corresponding author
Email address: mail@telenczuk.pl (Bartosz Teleńczuk)

mass activity of neurons located in small volume around the recording site (Einevoll et al., 2013). Although LFP is easy to record, it has proven notoriously difficult to interpret and model (Einevoll et al., 2013; Buzsáki et al., 2012). These difficulties partially originate from the complexity of neuronal coding (Denker et al., 2011; Saleh et al., 2012), but they also result from the very nature of the LFP signal, which represents the neuronal activity only indirectly through the flow of the extracellular currents (Einevoll et al., 2013; Bédard et al., 2004). This current flow depends on a number of parameters such as the neuronal morphology (Lindén et al., 2010), membrane ion channels (Reimann et al., 2013), electric properties of the tissue (Bédard et al., 2004), brain area and cortical layer (Lindén et al., 2011) impeding the interpretation of the resulting LFP signal.

We have begun to understand some of the cellular origins of the LFP signal (Buzsáki et al., 2012). In particular, simultaneous recordings of spiking activity and LFP have proven to be very useful in studying its generation (Teleńczuk and Destexhe, 2015). The relation of spikes to LFP can be studied, for example, using spike-triggered LFP average (st-LFP) (Teleńczuk et al., 2015), which estimates the LFP associated with each spike of a single neuron. Such measures have been used to asses gamma-band synchronisation between neurons (Gray and Singer, 1989), to detect spike locking to phase of oscillatory LFP (Destexhe et al., 1999), to characterise the synaptic connectivity (Swadlow et al., 2002) and to study travelling cortical waves (Nauhaus et al., 2009). In addition, the st-LFP is modulated by the waking state (Destexhe et al., 1999) and stimulus contrast (Ray and Maunsell, 2011). However, the direct LFP contributions of transmembrane and synaptic currents triggered by a single spike (unitary LFP) could not be identified, because st-LFP can not discern them from on-going LFP activity and recurrent activity in the network (Einevoll et al., 2013; Nauhaus et al., 2012).

In this study, we aimed to differentiate the contributions of interneurons and pyramidal neurons to LFP recorded from awake humans and non-human primates. We anticipated that the long-duration recordings with dense grid of electrodes (Utah array) (Peyrache et al., 2012; Dickey et al., 2009) will allow us to separate LFP components of putative interneurons and pyramidal neurons. Since cell morphology and connectivity affect the LFP (Lindén et al., 2010, 2011), we expected that these two types of neurons should be associated with diverse LFP contributions. We found that for both populations st-LFPs are dominated by spatially and temporally broad

components, which might correspond to non-causal relation with the population activity. We then estimated spatial filters adapted to the structure of on-going LFP, which allowed us to focus on the focal contributions instead. Using this methods we could demonstrate for the first time that the interneurons in comparison with pyramidal neurons, interneurons have a more dominant unitary contribution to local LFP.

2. Results

We investigated the local field potential (LFP) contribution associated with a single spike in human and non-human-primate cortex. The data were recorded from the temporal cortex of patients who underwent a surgical procedure for the localisation of the epileptic foci (Peyrache et al., 2012) and from the pre-motor cortex (PMd) of macaque monkey (Saleh et al., 2012) (Figure 1A). The LFP and spiking activity (Figure 1B) were recorded with a 10-by-10 array of intracortical electrodes (Utah array, interelectrode distance 400 μm). Spikes of single neurons were then discriminated by semi-automatic clustering (see Methods) and their relation to the LFP was estimated with the spike-triggered LFP average (st-LFP), that is the average of short LFP segments centered around each spike time. This procedure can be applied to LFP signals from all electrodes, but always keeping firing of the same neuron as the reference. Thus we obtained a spatio-temporal map of the LFP components coincident with a spike of a given neuron (Figure 1C).

The estimated st-LFPs are not confined to local neighbourhood of the trigger neuron, but they spread rapidly through the entire array (Figure 1C, middle and bottom). In addition, many components, even at distant electrodes, appear nearly simultaneously with a spike of the reference neuron or they even precede the spike. Such components decay with long spatial scale from the position of the neuron (Figure 1D-E). Such non-local and non-causal components can not be interpreted as the field generated directly by the active neuron (via the post-synaptic potentials), because most neurons synapse at distances no more than 1 mm (Holmgren et al., 2003; Levy and Reyes, 2012).

Thus the st-LFP can not be interpreted as the LFP contribution of post-synaptic currents triggered by a single spike either directly (mono-synaptically) or mediated through other neurons

(poly-synaptically). To explain the spatial and temporal spread of the st-LFP, we note that the spikes used to trigger the LFP average are generated within the network and that they are a by-product of extensive neuron-to-neuron correlations distributed spatially and temporally. In addition, many of the neurons share their synaptic inputs arriving from different brain areas, so that the st-LFP may also reflect the spatial distribution of synaptic projections and the time trace of the pre-synaptic currents. Finally, LFP captures signals electrically conducted by the neuronal tissue from other brain areas. Therefore, the spike-triggered LFP average extracts not only the contribution of the trigger neuron, but it sums all the pre- and post-synaptic currents from other neurons.

We developed a novel technique to recover the local contribution from the st-LFP. The technique is based on the notion that the LFP potentials triggered by a single neuron are superimposed on the baseline spatial correlations already present in the on-going LFP. Under this assumption we can remove the baseline by application of linear spatial filters, whose weights are adapted to the co-variance matrix of the on-going LFP. For correlation depending on space only through distance and not exact positions of the electrodes, the spatial filter would resemble the second spatial derivative (a laplacian) with the largest weights concentrated around the trigger electrode and its surroundings. The estimated filters adapted to the data manifest similar structure, but they also feature additional off-center components that are absent in the spatial derivative (Figure 2A).

Application of this method to st-LFP allowed to suppress the global components present in the entire array and keep only small components localised around the cell (Figure 2B, right). These components reach no further than 1 mm from the cell so they may originate from the synaptic currents directly evoked by the trigger neuron (Figure 2D, right). Similarly, spatial whitening recovered local LFP contributions in macaque pre-motor cortex (Figure 2E).

We compared the local st-LFP for the putative inhibitory (fast spiking, FS) and excitatory (regular spiking, RS) neurons discriminated on the basis of a spike waveshape (Peyrache et al., 2012; Dehghani et al., 2016) (Figure 2D). We found that in their close neighbourhood the FS neurons produced significantly stronger whitened st-LFP, but this amplitude difference diminished with distance (Figure 2D, right). This larger focal contributions of FS neurons could originate from denser spatial distribution of the synaptic terminals or the morphology of their axonal

collaterals as suggested by previous in vitro results (Bazelot et al., 2010). In contrast, we found that the raw st-LFP of RS and FS neurons were not significantly different (Figure 1D).

In addition, the whitened st-LFPs triggered by FS neurons peaked consistently before the RS-based st-LFPs (Figure 2D-E, cf. Figure 3). This difference could be explained by an extra di-synaptic contribution of the RS neurons: RS neurons would excite the inhibitory interneurons, which in turn would contribute to the LFP. In this model the shift in st-LFP latency reflects the delay due to synaptic transmission ($\approx$ 2 ms). Importantly, this explanation also accounts for the fact that the excitatory and inhibitory unitary LFPs have the same polarity. Identical conclusions were reached from unitary LFPs in hippocampal slices (Bazelot et al., 2010), which are thus entirely consistent with the present findings.

The latency of the st-LFPs averaged over electrodes equi-distant to the trigger neuron increased gradually with the distance (Figure 2A, left). This is shown more precisely when plotting the latency of the trough against the electrode distance from the trigger neuron (Figure 3A). The linear dependency between these measures is suggestive of propagation with constant speed, which can be estimated from the inverse slope of the linear fit. For the st-LFPs averaged over all neurons (Figure 2A) the estimated propagation speed was 2.84 m/s for FS and 0.77 m/s for RS; the difference between RS and FS was not significant (bootstrap test, $n = 1000$ repetitions, $p > 0.01$).

The propagation speeds might reflect both the synaptic propagation (axonal conduction times and synaptic delays), as well as the passive propagation of electric field through the medium and indirect correlations between neurons. To focus on the direct effects, we analysed the propagation in the whitened st-LFP. We found that the propagation was slower in whitened st-LFP in comparison to the raw st-LFP (human: 0.51 m/s for RS neurons, 0.63 m/s, FS; monkey: 1.08 m/s, RS, 1.72 m/s, FS; Figure 3B). This may be due to the fact that the spatial filtering removes the effects of currents passively conducted through the tissue (volume conduction), which can propagate much faster than the synaptically-transmitted signals (Bédard and Destexhe, 2012). The combination of the nearly instantaneous (volume-conducted), and delayed (synaptically-propagated) st-LFP components may explain the higher overall propagation velocity in the non-whitened st-LFP. Interestingly, the propagation speed after whitening is consistent with action potential propagation speed in unmyelinated fibers (Debanne et al., 2011),

which further confirms that the whitened st-LFP represents unitary LFPs.

3. Discussion

We studied the relationship between neuronal activity and its surrounding electrical field by means of simultaneous recordings of single-unit spikes and the LFP signal. We found that the spike-triggered LFP can be described by a local component, which reflects single-neuron activity, and a diffuse component related to the baseline LFP correlations. Data-driven spatial filters recovered the local LFP field of each cell, the unitary LFP, which spreads at distances consistent with cortical anatomy and connectivity. The amplitude, peak latencies and propagation of such unitary LFP depended on the type of the neuron (inhibitory vs excitatory) used as the trigger. Specifically, the inhibitory neurons provide the largest contribution to the LFP in their close neighbourhood (< 1 mm).

The spike-triggered LFP is an estimate of correlation between the (continuous) LFP signal and the (point-like) spike trains. As a correlation measure it can not differentiate the causal contributions of the spike and its post-synaptic consequences from the incidental correlations between LFP and spikes. In line with the argument, we identified st-LFP components that were both non-causal (i.e. preceded the spike onset) and non-local (appearing simultaneously in distant electrodes, Figure 1C). These components are not specific to the activity of the "trigger" neuron, but characterise the local population of neurons and electric properties of neural tissue (Einevoll et al., 2013).

Notwithstanding, we recovered the local correlates of spikes in the LFP using spatial filters adapted to the co-variance structure of on-going LFPs (Figure 2A-C). Similar techniques have been used as a pre-processing step of blind source separation methods (Hyvärinen et al., 2004) and to study neuronal responses to natural stimuli (Schwartz et al., 2006). There is also a similarity with the current source density method (CSD) for localising current sources of the LFP especially with the inverse CSD formulation (Pettersen et al., 2008; Łęski et al., 2011). An alternative, and possibly more direct, method of assessing the spike contribution to LFP consists in triggering a spike externally at random times (for example, by means of direct current injection) and recording the associated LFP signal. This technique might dissociate the times of spiking

from the neurons's synaptic inputs and activity of other neurons. However, such recordings in intact tissue are technically challenging and to the best of our knowledge have not yet been performed in monkey and humans.

The latency, propagation speed and the spatial extent of the whitened st-LFPs are consistent with the hypothesis that they measure the contribution of the post-synaptic currents initiated by the "trigger" spike (Figure 2 and 3). Alternatively, the axon-propagating action potential could produce similar LFP contribution, albeit at shorter spatial ranges constrained by the axonal arborisation (Mitzdorf, 1985). It has been also suggested that the LFP is at least partially generated by the dendritic spikes (Nicholson and Llinas, 1971), which could constitute another source of the observed st-LFP traces. The fact that the whitened st-LFP propagates with a different velocity, approaching unmyelinated axon propagation velocity, constitutes another evidence that it represents unitary LFPs.

Our results are consistent with the finding that the main contribution to the LFP in hippocampal slices (the unitary field potentials) is due to inhibitory neurons, while the contribution from excitatory neurons is mediated by interneurons, di-synaptically (Bazelot et al., 2010). Two of our findings suggest that these conclusions are valid for human and monkey: the putative inhibitory neurons produce larger signal in their close neighbourhood compared to the putative excitatory neurons; and the excitatory contribution to the LFP lags behind the inhibitory (Figure 2D-E). The latency difference might reflect an additional synaptic delay required for the di-synaptic activation of the mediating interneuron as suggested by Bazelot et al. (2010), but it was not as pronounced as reported in their in vitro study. It remains to be investigated whether this difference is specific to the experimental protocol of the present study (behaving awake subjects), preparation used (in vivo) or recorded brain area (pre-motor cortex and temporal cortex). In the present study, we can not directly address the origin of these cell-type differences. However, they are consistent with the differences in the morphologies of the neurons, most notably in the degree of axonal arborisation.

The spike-triggered LFP remains an essential method in answering how activities of single neurons are embedded in on-going rhythms (Ray and Maunsell, 2011). In addition, we demonstrated that it can be used to asses the specific contribution of the single neurons to the LFP and, indirectly, their synaptic connectivity. Future work might clarify whether this contribution is

specific to different brain areas, cortical layers or brain states and whether it might undergo dynamic changes during learning. Such an approach provides a new way to investigate the interactions between microscopic and macroscopic scales of cortical organisation.

4. Methods

4.1. Experimental methods

Human recordings were acquired from in-patient invasive monitoring of two patients with focal epilepsy. The neuroprobe (Utah array) was placed in layer II/III of the middle temporal gyrus. This array is silicon-based, made up of 96 microelectrodes with 400 μm spacing, covering an area of 4×4 mm. Data were sampled at 30 kHz (Cerebrus Blackrock Microsystems). Single units were discriminated by using standard clustering methods. The data was recorded under normal behaviour (no specific task was administered during this recording). The data were scored into awake and slow-wave sleep periods based on EEG and video recordings. The full experimental protocol can be found in Peyrache et al. (2012).

The monkey recordings were performed during the night in the pre-motor cortex of macaque monkey (Macaca mulatta) implanted with Utah arrays described above. During a recording session, signals from 96 electrodes were amplified (gain of 5,000), band- pass filtered between 0.3 Hz and 7.5 kHz, and recorded digitally (14-bit) at 30 kHz per channel using a Cerebus acquisition system (Blackrock Microsystems). Spike waveform data were sorted off-line (Plexon, Dallas, TX) using a user-defined template. All spike waveforms whose mean squared error from this template fell below a user-defined threshold were classified as belonging to that unit. The full experimental protocol can be found in Dickey et al. (2009).

We discriminated the putative regular-spiking (RS) and fast-spiking (FS) neurons based on their extracellular spike features. The details of the procedure for human and monkey data were described elsewhere (Peyrache et al., 2012; Dehghani et al., 2016).

4.2. Data analysis

We calculated the spike-triggered average of the LFP (st-LFP) in order to estimate the contribution of a single spike to LFP (Schwartz et al., 2006). First, we calculated the average of

short segments of the LFP centered around each spike time of a single trigger neuron. Next, we repeated this process across LFP electrodes to obtain a spatio-temporal st-LFP:

$$\text{st-LFP}_i(t) = \frac{1}{n_{\text{sp}}} \sum_{k=1}^{n_{\text{sp}}} \text{LFP}_i(t - t_k) \tag{1}$$

where $i = 1..96$ are the indices of the electrodes and $\{t_k\}_{k=1}^{n_{\text{sp}}}$ are all n_{sp} spike times of the trigger neuron. To avoid spike artifacts, the LFP signal for the electrode with spikes of the trigger neuron was removed from the data. For the purpose of visualisation (Figure 1C and Figure 2C) the missing electrodes were replaced with the average of neighbour electrodes.

We estimated the peak latencies in the population-averaged whitened st-LFP (Figure 3D-E) by finding the global minimum of the st-LFP in the time-window of [-10, 15] ms. To estimate the peak latency of single-neuron st-LFP (Figure 3A) we fitted an asymmetric Gaussian in the time range $[-10, 25]$ ms:

$$f(t) = y_0 + A \begin{cases} \exp\left(-(t-\delta)^2/\sigma_1^2\right) & \text{if } t \geq \delta \\ \exp\left(-(t-\delta)^2/\sigma_2^2\right) & \text{if } t < \delta \end{cases} \tag{2}$$

where the baseline y_0, the amplitude A, the left and right widths σ_1, σ_2 and the latency δ are fitted using nonlinear least-squares method (Levenberg-Marquardt algorithm).

To whiten the st-LFPs we first calculated the co-variance matrix of the on-going band-pass filtered (15 – 300 Hz) LFP signals $(\mathbf{C}_{\text{LFP}})_{ij} = \langle \text{LFP}_i(t)\text{LFP}_j(t) \rangle_t$ (where $\langle \cdot \rangle_t$ denotes temporal averaging). The whitening matrix $\mathbf{W}$ is calculated by the inverse square root of $\mathbf{C}_{\text{LFP}}$ (Hyvärinen et al., 2004):

$$\mathbf{W} = \mathbf{C}_{\text{LFP}}^{-1/2} = \mathbf{E}\mathbf{D}^{-1/2}\mathbf{E}^T, \tag{3}$$

where $\mathbf{E}$ is a matrix of eigenvectors of $\mathbf{C}_{\text{LFP}}$ and $\mathbf{D}$ is a diagonal matrix with inverse square roots of eigenvalues λ_i on its diagonal ($(\mathbf{D})_{ii} = 1/\sqrt{\lambda_i}$, $(\mathbf{D})_{ij} = 0$).

Given the matrix $\mathbf{W}$ the whitening operation amounts to the matrix product of $\mathbf{W}$ with the spike-triggered LFP:

$$\text{st-LFP}_i^w = \sum_{j=1}^{96} (\mathbf{W})_{ij} \text{st-LFP}_j \tag{4}$$

where st-LFP^{w}s are the whitened st-LFPs.

In pre-processing steps, the LFP signals were band-pass filtered 15 – 300 Hz. The filtering was applied in Fourier domain where its response was 1 for all frequencies in the pass-band and 0 in stop-band. To avoid ringing artifacts, at the corner frequencies the response decayed to 0 with a profile of a Gaussian with width of 10 Hz.

Acknowledgments

Research funded by Centre National de la Recherche Scientifique (CNRS, France), European Community Future and Emerging Technologies program (BrainScales FP7-269921; The Human Brain Project FP7-604102), National Institutes of Health (NIH grants 5R01NS062092, R01EB009282 and R01NS045853, R01MH099645) and Office of Naval Research (MURI grant number N00014-13-1-0672).

References

Bazelot, M., Dinocourt, C., Cohen, I., Miles, R., 2010. Unitary inhibitory field potentials in the CA3 region of rat hippocampus. J. Physiol. (Lond.) 588 (Pt 12), 2077–2090.

Bédard, C., Destexhe, A., 2012. Modeling local field potentials and their interaction with the extracellular medium. In: Brette, R., Destexhe, A. (Eds.), Handbook of Neural Activity Measurement. Cambridge University Press, Cambridge, pp. 136–191.

Bédard, C., Kröger, H., Destexhe, A., 2004. Modeling extracellular field potentials and the frequency-filtering properties of extracellular space. Biophys. J. 86 (3), 1829–1842.

Buzsáki, G., Anastassiou, C. A., Koch, C., 2012. The origin of extracellular fields and currents–EEG, ECoG, LFP and spikes. Nat. Rev. Neurosci. 13 (6), 407–420.

Debanne, D., Campanac, E., Bialowas, A., Carlier, E., Alcaraz, G., 2011. Axon Physiology. Physiol. Rev. 91 (2), 555–602.

Dehghani, N., Peyrache, A., Telenczuk, B., Le Van Quyen, M., Halgren, E., Cash, S. S., Hatsopoulos, N. G., Destexhe, A., 2016. Dynamic Balance of Excitation and Inhibition in Human and Monkey Neocortex. Sci. Rep. 6, 23176.

Denker, M., Roux, S., Lindén, H., Diesmann, M., Riehle, A., Grün, S., 2011. The Local Field Potential Reflects Surplus Spike Synchrony. Cereb. Cortex 21 (12), 2681–2695.

Destexhe, A., Contreras, D., Steriade, M., 1999. Spatiotemporal analysis of local field potentials and unit discharges in cat cerebral cortex during natural wake and sleep states. J. Neurosci. 19 (11), 4595–4608.

Dickey, A. S., Suminski, A., Amit, Y., Hatsopoulos, N. G., 2009. Single-unit stability using chronically implanted multielectrode arrays. J. Neurophysiol. 102 (2), 1331–1339.

Einevoll, G. T., Kayser, C., Logothetis, N. K., Panzeri, S., 2013. Modelling and analysis of local field potentials for studying the function of cortical circuits. Nat. Rev. Neurosci. 14 (11), 770–785.

Georgopoulos, A. P., Schwartz, A. B., Kettner, R. E., 1986. Neuronal population coding of movement direction. Science 233 (4771), 1416–1419.

Gray, C. M., Singer, W., 1989. Stimulus-specific neuronal oscillations in orientation columns of cat visual cortex. Proc. Natl. Acad. Sci. U.S.A 86 (5), 1698–1702.

Holmgren, C., Harkany, T., Svennenfors, B., Zilberter, Y., 2003. Pyramidal cell communication within local networks in layer 2/3 of rat neocortex. J. Physiol. (Lond.) 551 (Pt 1), 139–153.

Hyvärinen, A., Karhunen, J., Oja, E., 2004. Independent Component Analysis. John Wiley & Sons, New York.

Łęski, S., Pettersen, K. H., Tunstall, B., Einevoll, G. T., Gigg, J., Wójcik, D. K., 2011. Inverse current source density method in two dimensions: inferring neural activation from multielectrode recordings. Neuroinformatics 9 (4), 401–425.

Levy, R. B., Reyes, A. D., 2012. Spatial profile of excitatory and inhibitory synaptic connectivity in mouse primary auditory cortex. J. Neurosci. 32 (16), 5609–5619.

304 Lindén, H., Pettersen, K. H., Einevoll, G. T., 2010. Intrinsic dendritic filtering gives low-pass
305 power spectra of local field potentials. J. Comput. Neurosci. 29 (3), 423–444.

306 Lindén, H., Tetzlaff, T., Potjans, T. C., Pettersen, K. H., Grün, S., Diesmann, M., Einevoll,
307 G. T., 2011. Modeling the spatial reach of the LFP. Neuron 72 (5), 859–872.

308 Mitzdorf, U., 1985. Current source-density method and application in cat cerebral cortex:
309 investigation of evoked potentials and EEG phenomena. Physiol. Rev. 65 (1), 37–100.

310 Nauhaus, I., Busse, L., Carandini, M., Ringach, D. L., 2009. Stimulus contrast modulates
311 functional connectivity in visual cortex. Nat. Neurosci. 12 (1), 70–76.

312 Nauhaus, I., Busse, L., Ringach, D. L., Carandini, M., 2012. Robustness of traveling waves in
313 ongoing activity of visual cortex. J. Neurosci. 32 (9), 3088–3094.

314 Nicholson, C., Llinas, R., 1971. Field potentials in the alligator cerebellum and theory of their
315 relationship to Purkinje cell dendritic spikes. J. Neurophysiol. 34 (4), 509–531.

316 Pettersen, K. H., Hagen, E., Einevoll, G. T., 2008. Estimation of population firing rates and
317 current source densities from laminar electrode recordings. J. Comput. Neurosci. 24 (3),
318 291–313.

319 Peyrache, A., Dehghani, N., Eskandar, E. N., Madsen, J. R., Anderson, W. S., Donoghue, J. A.,
320 Hochberg, L. R., Halgren, E., Cash, S. S., Destexhe, A., 2012. Spatiotemporal dynamics of
321 neocortical excitation and inhibition during human sleep. Proc. Natl. Acad. Sci. U.S.A. 109 (5),
322 1731–1736.

323 Ray, S., Maunsell, J. H. R., 2011. Network rhythms influence the relationship between
324 spike-triggered local field potential and functional connectivity. J. Neurosci. 31 (35),
325 12674–12682.

326 Reimann, M. W., Anastassiou, C. A., Perin, R., Hill, S. L., Markram, H., Koch, C., 2013. A
327 biophysically detailed model of neocortical local field potentials predicts the critical role of
328 active membrane currents. Neuron 79 (2), 375–390.

329 Saleh, M., Takahashi, K., Hatsopoulos, N. G., 2012. Encoding of coordinated reach and grasp
330 trajectories in primary motor cortex. J. Neurosci. 32 (4), 1220–1232.

331 Schwartz, O., Pillow, J. W., Rust, N. C., Simoncelli, E. P., 2006. Spike-triggered neural
332 characterization. J. Vision 6 (4), 484–507.

333 Swadlow, H. A., Gusev, A. G., Bezdudnaya, T., 2002. Activation of a cortical column by a
334 thalamocortical impulse. J. Neurosci. 22 (17), 7766–7773.

335 Teleńczuk, B., Baker, S. N., Kempter, R., Curio, G., 2015. Correlates of a single cortical action
336 potential in the epidural EEG. Neuroimage 109, 357–367.

337 Teleńczuk, B., Destexhe, A., 2015. Local field potential, relationship to unit activity. In: Jaeger,
338 D., Jung, R. (Eds.), Encyclopedia of Computational Neuroscience. Springer, New York, pp.
339 1579–1584.

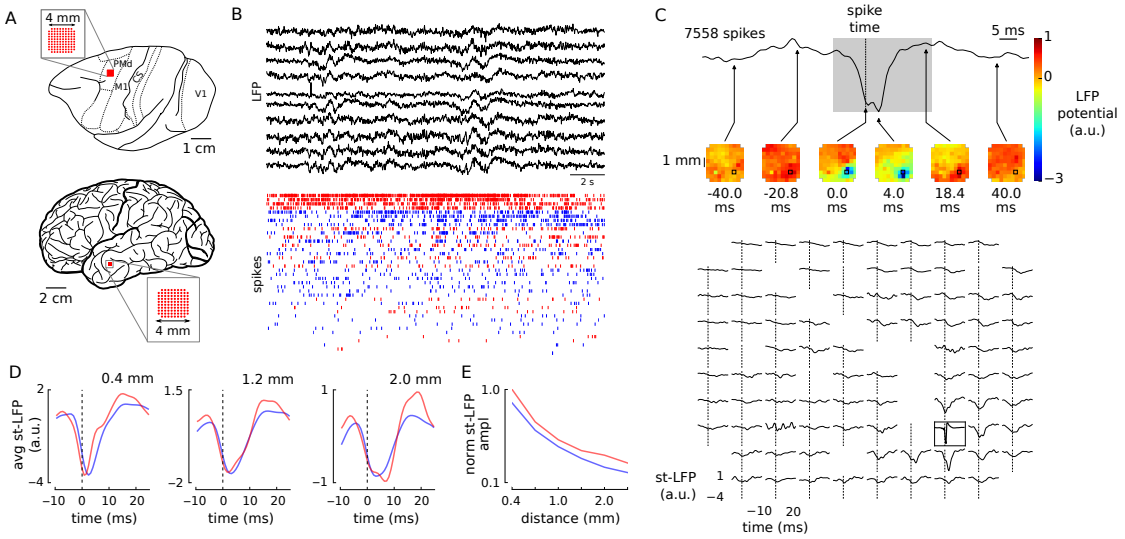

Figure 1: **Spikes of single neurons are associated with spatially diffuse and non-causal LFP patterns.** (**A**) Local field potentials and spikes were measured in the premotor cortex of macaques (top) and temporal cortex of human subjects (bottom) using Utah arrays. (**B**) LFP (top, subset of LFPs recorded simultaneously from macaque pre-motor cortex) and spikes (bottom, subset of neurons) obtained from Utah array. Neurons were classified into regular spiking (bottom, blue) and fast spiking (red) types based on spike waveshape. (**C**) Spatio-temporal spike-triggered LFP average (st-LFP) in human temporal cortex. *Top*: Average of the st-LFPs (band-pass filtered 15 – 300 Hz, average of 7558 spike-triggered segments) from the electrodes neighbouring with the trigger neuron. *Middle*: A color map of st-LFP amplitudes at selected time lags around the spike. The values for missing electrodes were linearly interpolated. *Bottom*: The st-LFP from all valid electrodes of the array plotted in time (plotting window adjusted to the gray-shaded segment in top panel). The st-LFP at the neuron position (black rectangle) was replaced with the spike waveform (amplitude normalised). Most st-LFPs express non-causal components preceding the spike (spike onset shown with vertical dotted line). (**D**) st-LFPs averaged for all electrodes separated from the trigger neuron with same distance (3 distances: 0.4 mm, 1.2 mm, 2 mm shown from left to right) and for all neurons classified as inhibitory (red) or excitatory (blue). (**E**) The st-LFP trough amplitude as a function of the distance from neuron to LFP electrode.

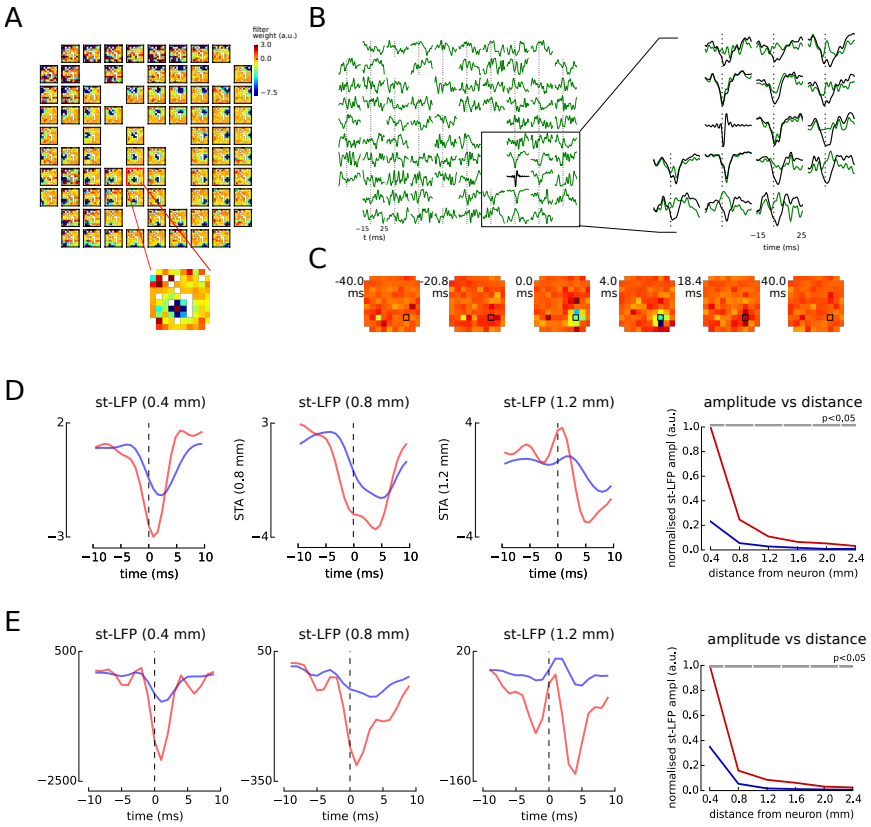

Figure 2: **The focal LFP of fast spiking (FS) and regular spiking (RS) neurons recovered by spatial decorrelation (whitening).** (**A**) Spatial filters designed to decorrelate (whiten) the LFP signals. Colors show filter weights associated with each electrode. *Inset*: Scaled-up heatmap of weights to whiten a single st-LFP (single row of whitening matrix). (**B**) Whitened st-LFPs of a single neuron shown in prior (black) and after whitening (green). *Right*: close-up of the whitened st-LFPs enclosed in black rectangle. Most st-LFPs are suppressed after spatial whitening and only st-LFPs directly adjoining the neuron are conserved. (**C**) Spatial maps of whitened st-LFP (top, compare with Figure 1C). (**D**) The population-averaged st-LFPs after whitening for human. Whitened st-LFPs averaged across neurons and electrodes at three distances from the trigger neuron (0.4 mm, 0.8 mm, 1.2 mm; compare with Figure 1D). st-LFP trough amplitude as a function of the distance between the neuron and LFP electrode (cf. Figure 1E). The gray horizontal bars at the top indicate significant differences between RS and FS neurons (bootstrap test, $p < 0.05$). The st-LFPs triggered on spikes of fast spiking neurons (red) are of higher amplitude and faster spatial decay (right-most panel). (**E**) Same as (D) for monkey.

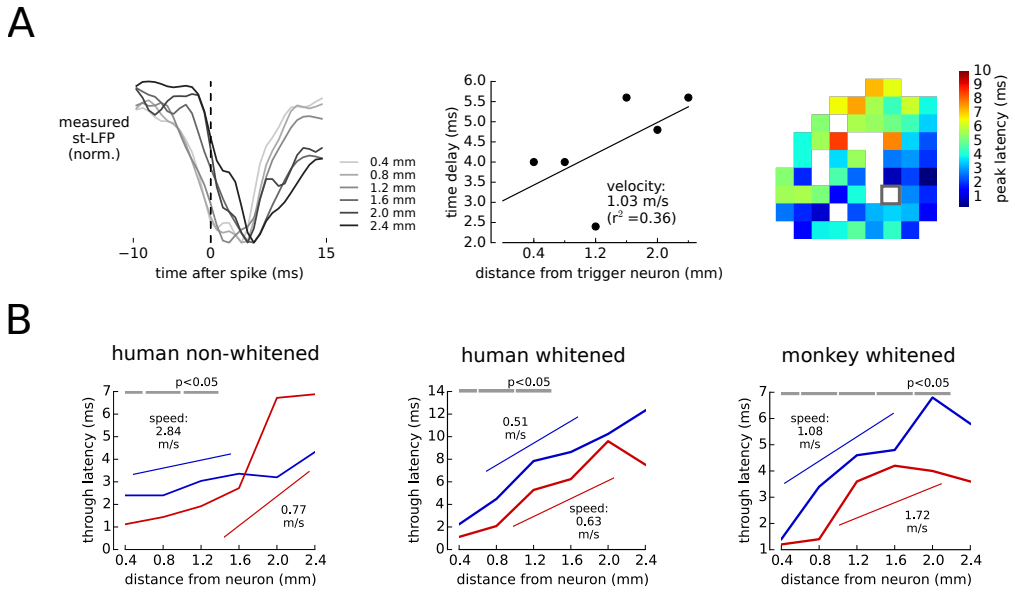

Figure 3: **st-LFPs propagate across cortex**. (**A**) Propagation of the raw st-LFP across the electrode array. *From left to right*: single-neuron st-LFPs averaged over all electrodes with the same distance from the trigger neuron; the latency of averaged st-LFP troughs (dots) and the linear fit (solid line); the latency of st-LFPs from each electrode as a heatmap (blank squares are due to missing electrodes or absence of pronounced st-LFP trough). The latencies increase with the distance supporting the hypothesis of spike-evoked LFP propagation. (**B**) The propagation of population-averaged traces. The trough latencies of whitened st-LFPs shown in Figure 1D (left), 2C (middle) and 2D (right) increase with distance. In whitened st-LFPs the RS latencies are consistently larger than FS at all distances (horizontal bars indicate significant difference between RS and FS neurons, bootstrap test, $p < 0.01$). The propagation velocity estimated from the inverse slope of the linear fit (thin line) is faster in raw human st-LFP (left) than the whitened human st-LFP (middle). The difference in propagation speeds between FS and RS neurons is not significant (bootstrap, $p > 0.01$)